Available online at www.sciencedirect.com

ScienceDirect

Procedia IUTAM 26 (2018) 30–42

Procedia IUTAM

www.elsevier.com/locate/procedia

IUTAM Symposium Wind Waves, 4–8 September 2017, London, UK

Wind-Wave Breaking

W. Kendall Melville*

Scripps Institution of Oceanography, U.C. San Diego, 9500 Gilman Dr., La Jolla, CA 92093-0213, USA

Abstract

Rational models of wind-wave growth were proposed in the 1950s (Miles 1957, Phillips 1957), theories of wave-wave interactions (Phillips 1960, Hasselmann 1962, Zakharov 1968) and wave-action conservation for waves in fluids (Whitham 1965, Bretherton and Garrett 1969) in the 1960s, but it was not until the 1980s that laboratory experiments (Duncan 1981, Melville and Rapp 1985) and a seminal paper by Owen Phillips in 1985 on a model of the equilibrium range in wind-wave spectra, and a formulation of breaking, began a rational program of research into the role of breaking in surface wave kinematics and dynamics. Two important features of Phillips' 1985 paper were the introduction of $\Lambda(c)dc$, the average total length of breaking fronts per unit area of ocean moving with velocities in the range (c, c + dc) and the statement that the average rate of energy loss per unit area by breakers in the same velocity range was given by

$$\varepsilon_b(c)dc = b(c)\rho g^{-1}c^5\Lambda(c)dc$$

where b is a dimensionless breaking strength and g is gravity. The energy loss per unit length of breaker, $b\rho g^{-1}c^5$, was based on Duncan's work, but anticipated in part by Lighthill (1978). Lower order moments of $\Lambda(c)$ describe kinematical features of breaking up to the third moment, with the fourth moment describing the momentum flux from waves to currents. The structure of the dissipation equation imposes a combination of different approaches to quantifying it. Estimates of b have depended on arguments based on Taylor's (1935) inertial scaling of turbulence dissipation, supported by laboratory experiments and recent DNS and LES numerical experiments, while $\Lambda(c)$ over any significant dynamical range can only be measured in the field. The success of the early attempts to follow this approach has led to recent work on air entrainment for gas transfer, and theoretical uses of fundamental vortex dynamics to develop our knowledge of the role of breaking in air-sea interaction. In this paper I will review the material from the laboratory, through scaling arguments, modeling and field measurements.

Peer-review under responsibility of the scientific committee of the IUTAM Symposium Wind Waves.

* Corresponding author. Tel.: +1-858-534-0478; fax: +1-858-534-7132.
E-mail address: kmelville@ucsd.edu

2210-9838
Peer-review under responsibility of the scientific committee of the IUTAM Symposium Wind Waves.
10.1016/j.piutam.2018.03.004

Keywords: Wind waves; wave spectra; wave breaking; breaking statistics.

1. Introduction

Modern studies of wave breaking in deep water have accelerated significantly since the 1980s. Early modeling of wave breaking was essentially a tuning exercise to maintain consistency with parts of the physics that were thought to be better understood: i.e. the wind input to the wave field and the nonlinear four-wave interactions. Much of the progress on breaking has been due to the influence of Owen Phillips' 1985 paper on the equilibrium spectrum of wind waves and his seminal ideas on the formulation and statistics of the breaking problem. Progress has proceeded through laboratory experiments, scaling arguments, theory, numerical modeling and field work, with the latter depending to a great extent on instrument development in both the laboratory and the field. While there appears to have been significant progress, many problems remain. Furthermore, it is likely that as our understanding of breaking improves it will point to weaknesses in other areas of wind-wave science.

Breaking limits the height of surface waves, mixes the ocean surface, generates currents, and enhances air-sea fluxes of heat, mass and momentum through the generation of turbulence, the entrainment of air and the creation of spray and aerosols. Breaking is a transition process from pure wave dynamics, which may be considered laminar, to two-phase turbulent flow dynamics. In the field these patches of turbulence are intermittent in space and time, and depend, in ways that are yet not completely understood, on the group statistics of the wave field. Figure 1 shows examples of wind-forced breaking wave fields off the coast of California.

In this paper I provide a brief review of work done by my research group on the title problem using laboratory and field experiments, theory and numerical work. A more complete review of the topic is beyond the constraints of these conference proceedings. Despite the complexity of the breaking problem, we find that progress has been made on understanding the kinematics and dynamics. While this progress depends on advances in observational and DNS numerical techniques, it also depends on the use of classical scaling arguments from turbulence theory.

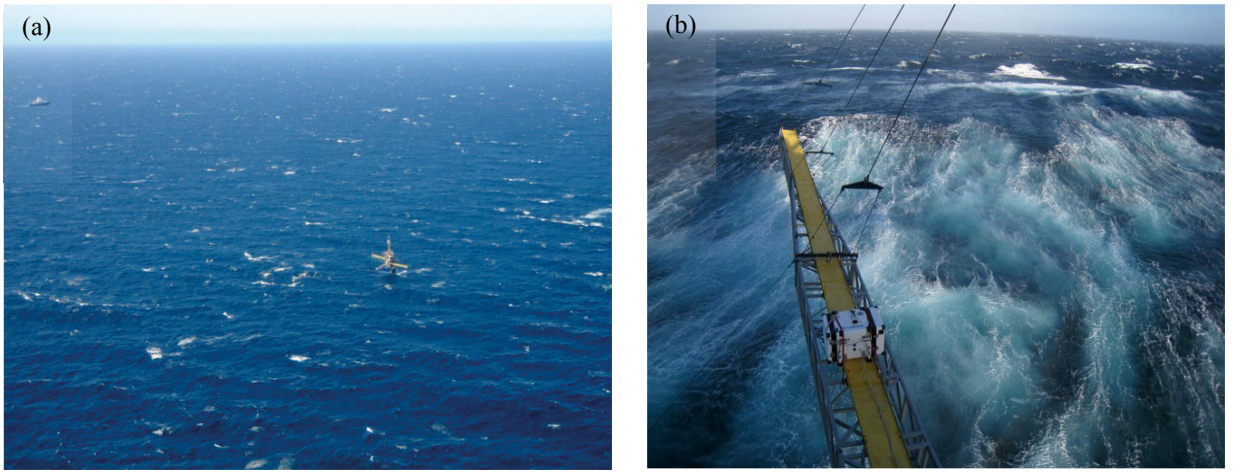

Figure 1. (a) left: Breaking wave field off S. California, March 2017. Note R/P FLIP (centre) and R/V Sally Ride (top left). (b) right: Rear face of a breaking wave taken from FLIP off N. California, June 2010. FLIP's boom is approximately 20 m long. Photo credit: Nick Statom.

2. Phillips (1985) model

2.1 The Wave Field

Before considering breaking it is important to describe the underlying wave field. Phillips (1985) started with the radiative transfer equation

$$\frac{dN}{dt} = \frac{\partial N}{\partial t} + (\mathbf{c}_g + \mathbf{U})\mathbf{g}\nabla N = \frac{S_{in} + S_{nl} + S_{ds}}{\sigma} , \tag{2.1}$$

where N is the wave action, $\mathbf{c}_g$ is the group velocity, $\mathbf{U}$ the current, S_{in} the wind input, S_{nl} the nonlinear wave-wave interaction, S_{ds} the dissipation due to breaking and σ the intrinsic frequency. The energy "source" terms comprise the numerator on the right-hand side of equation (2.1). If dN/dt is slow enough, then to leading order Phillips assumed equilibrium, that is

$$S_{in} + S_{nl} + S_{ds} = 0 , \tag{2.2}$$

and that all three "source" terms were of comparable magnitude and proportional to one another. With these assumptions he found that the directional wave spectrum was given by

$$\Psi(\mathbf{k}) = k^{-4} B(\mathbf{k}) = \beta(\cos\theta)^p u_* g^{-1/2} k^{-7/2}, \quad p \sim 1/2 , \tag{2.3}$$

with an omnidirectional spectrum proportional to $k^{-5/2}$ and a frequency spectrum $\Phi(\sigma) = \alpha g u_* \sigma^{-4}$. Here $\mathbf{k}$ is the vector wavenumber, $k = |\mathbf{k}|$, $B(\mathbf{k})$ is the saturation of the wave spectrum and u_* is the friction velocity in the marine atmospheric boundary layer. Figure 2 shows recent data with the $k^{-5/2}$ equilibrium spectrum followed by a k^{-3} saturation spectrum, measured by airborne lidar, and the corresponding frequency spectrum measured from FLIP (Lenain & Melville, 2017)

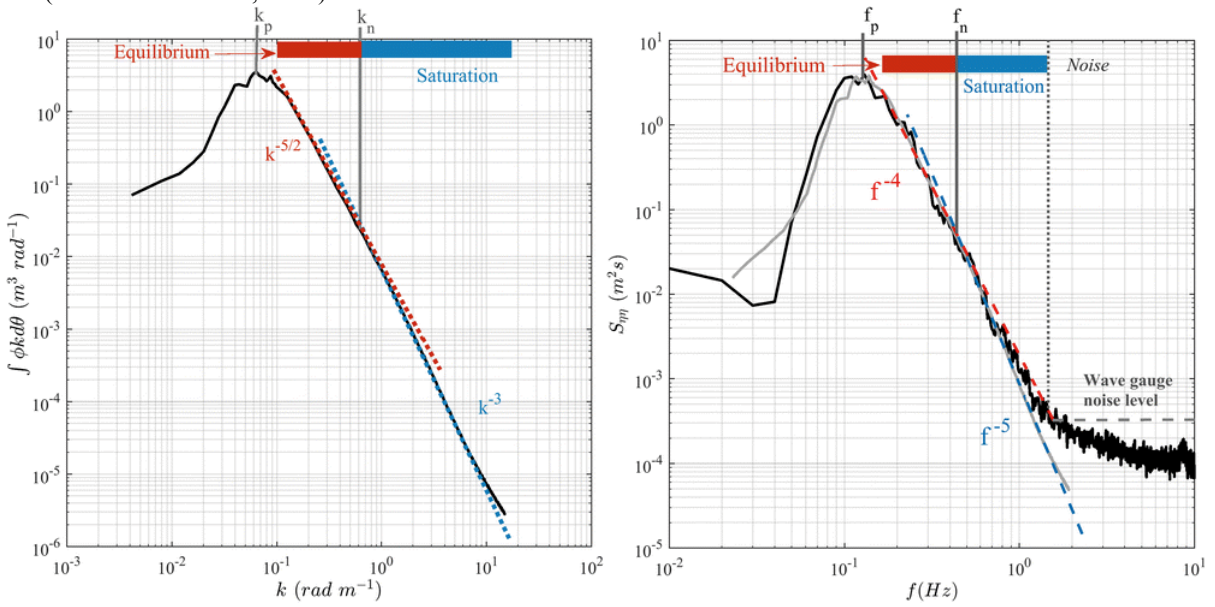

Figure 2. Wind-wave wavenumber (left) and frequency (right) omnidirectional spectra (Lenain & Melville 2017).

2.2 Breaking statistics

Phillips defined the average length of breaking fronts per unit area of ocean surface moving with velocities in the range $(\mathbf{c}, \mathbf{c} + d\mathbf{c})$ by $\Lambda(\mathbf{c})d\mathbf{c}$. The fraction of surface turned over by breaking per unit time is then $R = \int c\Lambda(c)dc$, where $c = |\mathbf{c}|$. Following Duncan (1981) the average rate of wave energy loss by breakers per unit area of ocean surface is given by the fifth moment of Λ:

$$\varepsilon_b(c)dc = b\rho g^{-1} c^5 \Lambda(c)dc \tag{2.4}$$

where $\varepsilon_b dc$ is the dissipation due to breaking in $(c, c + dc)$ and b is a dimensionless strength of breaking (the "breaking parameter").

The related momentum flux from waves to currents is

$$m_b(\mathbf{c})d\mathbf{c} = b\rho g^{-1}c^4\Lambda(\mathbf{c})d\mathbf{c}. \tag{2.5}$$

In the equilibrium model,

$$\Lambda(\mathbf{c}) \propto b^{-1}(\cos\theta)^{3p}u_*^3 gc^{-7} \text{ while } \Lambda(c) \propto c^{-6}. \tag{2.6}$$

2.3 What is c?

Phillips (1985) assumed, but did not explicitly state, that c is the characteristic linear phase speed of the breaking wave. This was based on the quasi-steady experiments of Duncan (1981), in which geometric similarity of the breaking region relative to the underlying wave was found. This requires that c be the phase speed. Early breaking criteria assumed it was associated with Stokes limiting wave form for which the phase speed is approximately 9% more than the linear value; however, as shown below, the speed of the unsteady breaking fronts is typically O(10%) less than a characteristic linear phase speed for the group and can lead to significant differences due to the importance of higher order moments of $\Lambda(c)$. In what follows we will use $c = (gk^{-1})^{1/2}$ to represent the linear phase speed of gravity waves and $c_b = |\mathbf{c}_b|$ to represent the speed of the breaking front.

3. Generating breaking in the laboratory.

Field data (Terrill & Melville 1988) shows that breaking of the dominant waves correlates with the wave groups. Laboratory data (Melville 1982, 1983) shows that Benjamin-Feir instability also leads to breaking by dispersive focusing following the amplitude and frequency modulation of the waves resulting from the B-F instability. The latter breaking is very gentle with no significant air entrainment and may be associated with the generation of dissipative parasitic capillaries. Longuet-Higgins (1974) suggested the use of the focusing of dispersive wave packets as a means of generating breaking in the laboratory and this technique has been exploited by Melville & Rapp (1985), Rapp & Melville (1990) and others to do controlled experiments on breaking. Figure 3 shows an x-t diagram of the focusing of the incident waves, the various phenomena resulting from breaking, and the path of the transmitted waves. Since the incident and transmitted waves become linear far enough upstream and downstream of breaking, x_1 and x_2 respectively, then equipartition applies and, since the radiated waves are found to be negligible, it is a relatively simple matter to measure the energy lost from the wave field due to breaking.

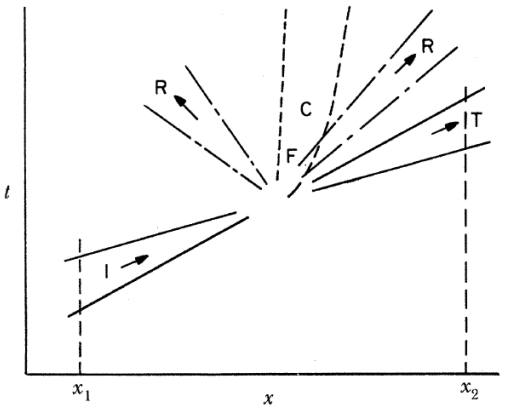

Figure 3. Schematic of focusing waves packet: I=incident waves, T=transmitted waves, R=radiated waves, C=current, F=turbulence (Rapp & Melville 1990).

Rapp & Melville (1990) used the dispersive focusing method to generate breaking of wave groups. By spreading dye over the surface pre-breaking and imaging the evolution of the dye during breaking, both c_b and the mixing down of the surface layer by breaking could be measured. Figure 4 shows examples of such an analysis where the initial value of $c_b = 0.8c$, and c is a characteristic phase speed of the waves in the group.

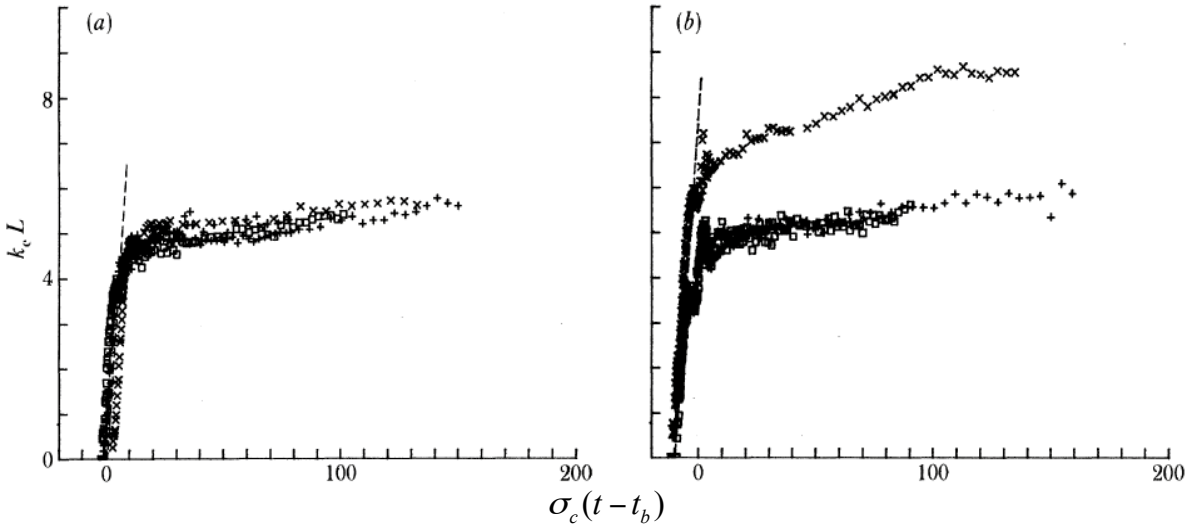

Figure 4. Non-dimensional length of surface mixed by breaking as a function of dimensionless time where (σ_C, k_C) are the center frequency and wavenumber and t_b is the linear prediction of time to focusing for (a) spilling wave and (b) plunging waves. Wave group centre frequency $f_C = 0.88$ Hz (×), 1.08 (+), 1.28 (W) and $\Delta f / f_C = 0.73$; $x_b k_c = 27.4$. The dashed lines correspond to a speed of $0.8c_c$.(Rapp & Melville 1990)

4. Wave energy dissipation

One of the overarching goals of breaking research is to measure or infer the wave energy dissipation in the field and use the results to improve the dissipation component of wind-wave models. We can write this dissipation as

$$S_{ds} = \int b\rho g^{-1} c^5 \Lambda(c) dc \tag{4.1}$$

where the breaking parameter, b, can be measured in the laboratory (Drazen et al. 2008), but $\Lambda(c)$ must be measured in the field since it is generally not possible to reproduce the dynamic directional range of the surface wave field in the laboratory. As mentioned above, breaking is a transition process, from wave motion to turbulence. Now one of the cornerstones of turbulence theory is G.I. Taylor's (1935) inertial model of dissipation: $\varepsilon = \chi u^3 / l$, where χ is a constant of O(1), u is an integral velocity scale and l an integral length scale, and the Reynolds number $\mathrm{Re} = ul/\nu$? 1. If we consider a plunging breaking wave as shown in Figure 5, the toe of the breaker travels at a ballistic velocity. If we assume that Taylor's inertial result applies, now with the initial wave variables rather than the integral turbulence scales, then we have a length scale from the vertical distance the toe of the breaker travels before hitting the surface, h, and the ballistic vertical velocity at impact , $w = (2gh)^{1/2}$. The inertial approach was initially considered by Melville (1994) who erroneously chose the incorrect initial velocity scale. The approach was subsequently followed by Drazen et al. (2008) who showed that the dissipation rate per unit length of breaking front was given by

$$\varepsilon_l = b\frac{\rho c^5}{g}; \tag{4.2}$$

here c *is* a characteristic phase speed, and

$$b = \beta(hk)^{5/2} \tag{4.3}$$

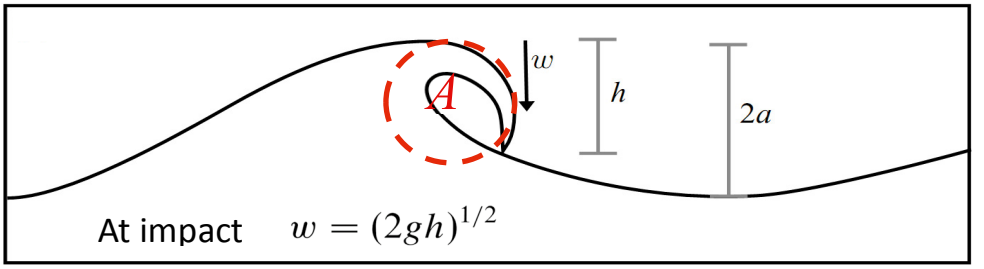

Figure 5. Schematic figure for inertial estimate of wave dissipation due to a plunging breaker. Red circle diameter h corresponds to area A of inertial dissipation. (Drazen et al. 2008)

Note that β is an O(1) constant and hk is a slope parameter with k a characteristic wavenumber. Drazen et al. (2008) found that laboratory experiments for strong breaking waves gave $b \propto (hk)^{5/2}$ within the scatter of the data. The disadvantage of this result, is that it is expressed in terms of hk a measure of the wave slope at breaking, something we do not know a priori. However, it was found that by using the linear prediction of the slope at focusing, S, that the best fit to the data was $b \propto S^{2.77}$, close to the 5/2 result. Subsequently, Romero et al. (2012) showed that by using a threshold slope, or offset, all the known laboratory measurements of b at that time could be accounted for by $b = 0.4(S - 0.08)^{5/2}$. These measurements ranged from incipient breaking to plunging waves over three orders of magnitude of b. This result is shown in Figure 6, where a cubic fit to the data is also shown, but one that is purely empirical with no physical foundation as is the case for $b \propto S^{5/2}$. Since these laboratory results were established, DNS (Deike et al. 2015, 2016, 2017) and LES (Derakhti & Kirby 2016: DK2016) have shown similar results, with the LES (DK2016, Fig. 14) showing that the use of a spectrally weighted slope, S_{so}, rather than S reduced the scatter about the curve $b = 0.3(S_{so} - 0.07)^{5/2}$.

Romero et al. (2012) used lidar measurements of the fetch-limited wave field in the Gulf of Tehuantepec (Romero & Melville (2010a,b) and simultaneous airborne video measurements of the whitecap kinematics to infer $\Lambda(c)$ (Kleiss & Melville 2010, see below) to see whether the laboratory measurements of b could be used to close the radiative balance equation, neglecting the currents and balancing the advective term by the source terms:

$$\begin{aligned} S_{ds}(x,k) &= c_g \cdot \nabla\Psi(x,k,\theta) - S_{in}(x,k) - S_{nl}(x,k) \\ \rho_w g S_{ds}(c)dc &= b\rho_w g^{-1} c^5 \Lambda(c) dc \end{aligned} \tag{4.4}$$

Since the mean square slope $mss = \int B(k)k^{-1}dk$, where $B(k) = \int \Psi(\mathbf{k})k^4 d\theta$ is the saturation, in defining the breaking strength b in the spectral model, Romero et al. (2012) used $b = A(B(k)^{1/2} - B_T(k)^{1/2})^{5/2}$. They found that in order to close the equations that they had to extrapolate $\Lambda(c)$ to values of c lower than those reliably measured by using whitecap kinematics (See dashed line in Figure 7a). The inference of this result was that the dynamics depended on breakers for which there was little or no significant air entrainment, certainly less than could be measured by airborne visible imagery.

5. Field measurements of breaking

5.1 Field measurements of $\Lambda(c)$

The need to measure both air-entraining and non-air-entraining breakers has introduced the need to use both visible and infrared (IR) imagery to measure the kinematics of the breaking. Evaporative cooling of a thin surface layer even by a slight wind means that when a wave gently breaks without significant air entrainment that cool skin is broken and is visible in the IR imagery.

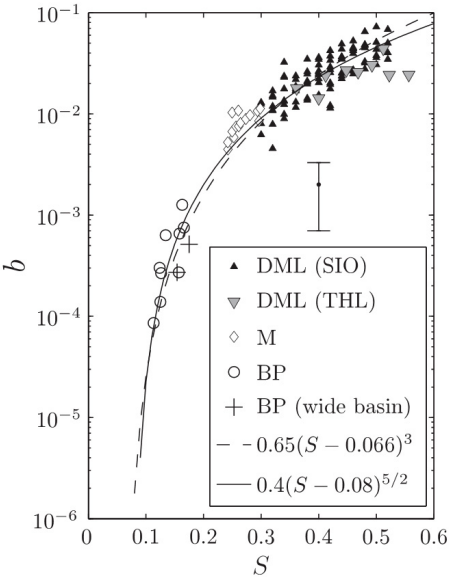

Figure 6. Breaking strength parameter b as a function of the linear prediction of the wave slope at breaking, S (Romero et al. 2012)

In a series of experiments from the research platform FLIP, Sutherland and Melville (2013; SM2013) used visible and IR imagery to measure $\Lambda(c)$ and acoustic Doppler instruments to measure the energy dissipation rate in the surface layers of the ocean. Figure 7 shows their $\Lambda(c)$ data, color coded by wave age, along with field data by others (Melville & Matusov 2002, Gemmrich et al. 2008, Phillips et al. 2001, Kleiss & Melville 2010), and laboratory measurements by Jessup & Phadnis (2005). Also shown are the predictions of Romero et al. (2012) based on the Kleiss & Melville (2010) $\Lambda(c)$ data from airborne visible imagery. The wave-age colour-coded SM2013 data generally show a decrease in $\Lambda(c)$ as the wave age increases. There was good agreement with Zappa et (2012) in measuring $\Lambda(c)$ with visible imagery from FLIP. Using dimensional analysis, and assuming the fetch dependence was included in other variables, Sutherland & Melville (2013) found that

$$\Lambda(c)\frac{c_p^3}{g}\left(\frac{c_p}{u_*}\right)^{0.5} = f\left(\frac{c_b}{\sqrt{gH_s}}\left\{\frac{gH_s}{c_p^2}\right\}^{0.1}\right) \tag{5.1}$$

provided a collapse of their data as shown in going from Figure 7a to Figure 7b. While they included the dependence on (gH_s/c_p^2), it is so weak as to be negligible within the scatter of the data. (Note that in Figures 7-9 from the papers of Sutherland and Melville, c is equivalent to our c_b.)

Sutherland & Melville (2013) also examined the relationship between the measurements of the wave energy dissipated by breaking and modeling of dissipation by Romero & Melville (2010b) where the dissipation term was based on Alves & Banner (2003) but explicitly forced saturation at the higher wavenumbers. The measured breaking- induced momentum flux from waves to currents was compared with the measured wind stress. These results are shown colour-coded by wave age in Figures 8a and 8b, respectively. It is clear from the figure that there is good agreement between the dissipation and momentum flux inferred from the $\Lambda(c)$ measurements and the

modeling (for dissipation) or wind stress (momentum flux) at the lower wave ages up to full development. However, both show differences for the largest wave ages, when the underlying waves are swell. Firstly, the differences at the larger wave ages might be expected since we do not expect much, if any, significant breaking of the swell. Secondly, we expect a significant correlation between the momentum and energy fluxes, **M** and E respectively, since they are related by

$$\mathbf{M} = \frac{\mathrm{E}}{c}\frac{\mathbf{k}}{k}. \tag{5.2}$$

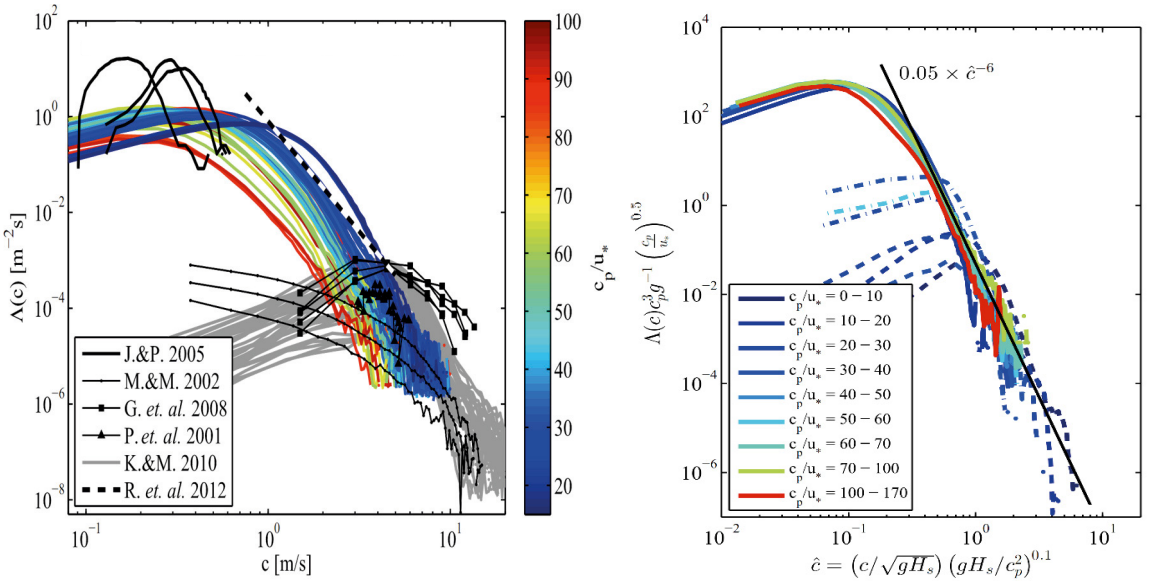

Figure 7. (a) left: Field and laboratory data and prediction described in the text. (b) right: Collapse of the SM2013 data with non-dimensional variables. (Sutherland & Melville 2013)

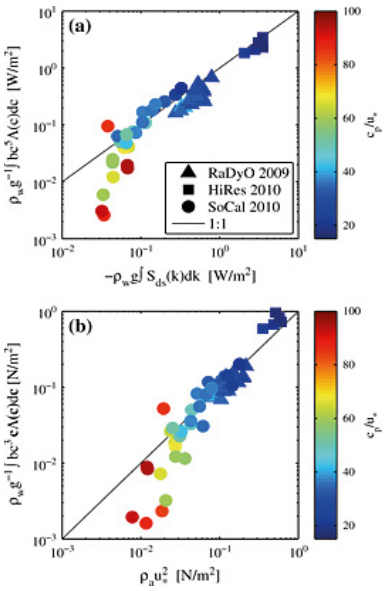

Figure 8. (a) Dissipation by breaking (ordinate) compared with modeled wave field dissipation (abscissa). (b) Momentum flux from waves to currents due to wave breaking (ordinate) plotted against wind stress (abscissa). Color shows wave age and solid line indicates 1:1 correspondence. (Sutherland & Melville 2013)

It is important to remember that the momentum flux from the atmosphere to the ocean, and the flux from the waves to currents are not necessarily locally equal. For example, some swell from Southern Ocean storms ends up providing momentum for wave set-up and along-shore currents on the beaches of the US west coast.

5.2 Field measurements of turbulent dissipation, ε

It has been known for some time that the dissipation rate per unit mass, ε, in the near-surface waters may be

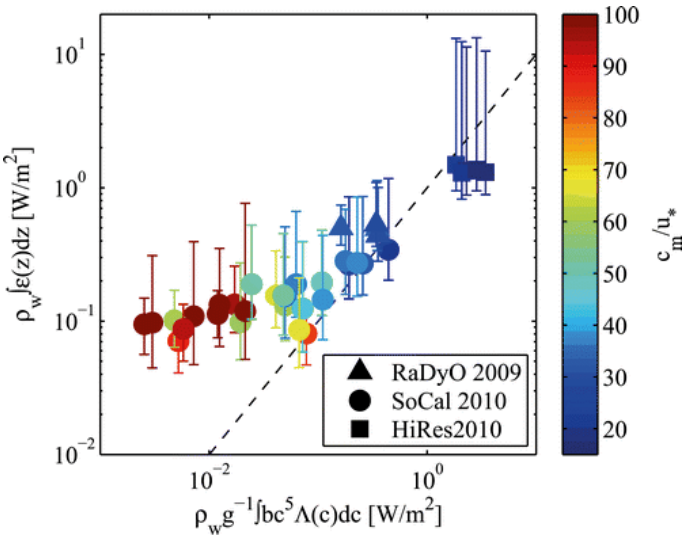

one Figure 9. Comparison between dissipation measured in the water column (ordinate) and by breaking (abscissa).(Sutherland & Melville 2015a)

to two orders of magnitude greater than that in the classical boundary layer over a rigid surface (Kitaigorodski et al.1983, Agrawal et al. 1992). In that classical case $\Phi_\varepsilon \equiv \varepsilon \kappa z / u_{*w}^3 = 1$ applies in the logarithmic law-of-the-wall region where κ is the von Karman constant, z is the distance from the surface and u_{*w} is the friction velocity in the water. The early measurements were not able to sample the data between wave troughs and crests but using acoustic Doppler techniques Gemmrich (2010) was able to reach within O(1) cm of the surface from below and found that the dissipation correlated with the wave spectrum saturation, a measure of breaking investigated by Banner et al. (2002). Sutherland & Melville (2015a) were able to measure dissipation in the water column using acoustic instrumentation and at the surface using stereo IR imagery from above (Sutherland & Melville (2015b). Over short intervals the sea surface temperature may be considered a passive tracer and so the velocity of the surface fluid can be measured using image processing techniques. See Figure 9.

6. Wave-current interaction and breaking

In what we have discussed so far we have just considered breaking in the context of a wind-forced wave field in the absence of inhomogeneous unsteady currents. However, it is well-known that waves propagating into an opposing current steepen, shorten and may break. This is most commonly seen in the nearshore when waves incident on the coast meet a river outflow on the ebb tide; however, the same physics is at play in deep water current systems when wind waves or swell meet opposing currents, extreme and breaking waves may be generated. This is the case in the Agulhas current and other major western boundary currents. There is also growing evidence of wave-current interaction leading to breaking at oceanic fronts as is shown in Figure 10. See Romero et al. (2017)

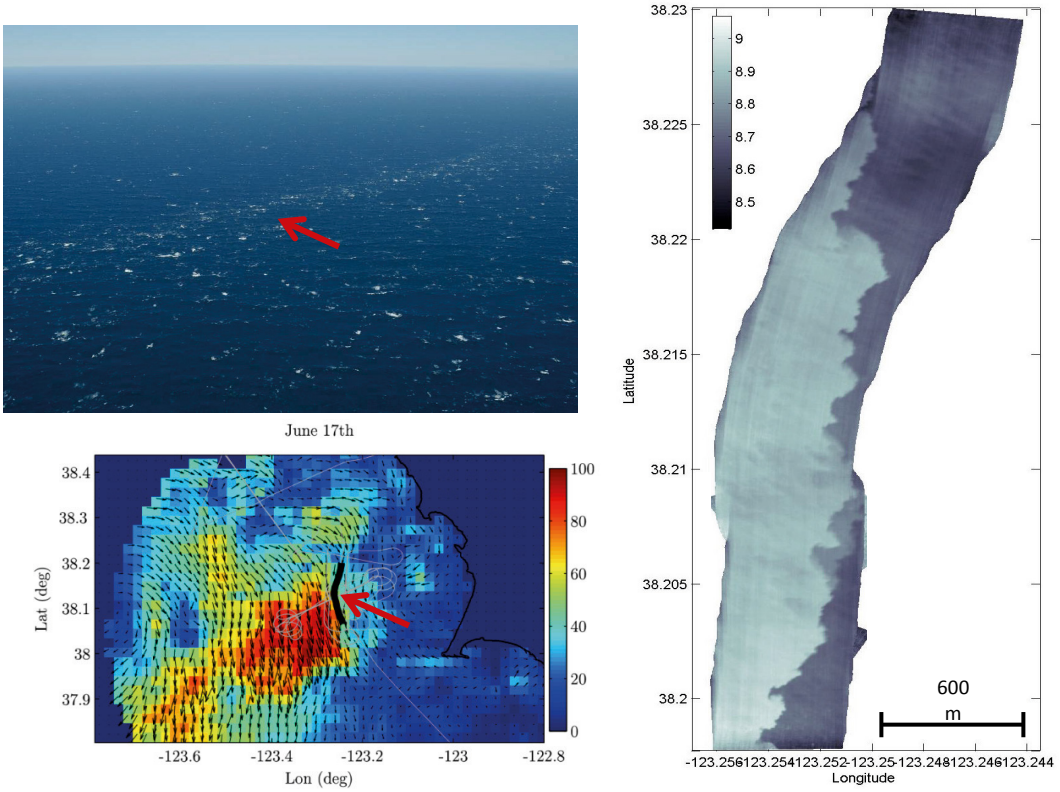

Figure 10. Clockwise from top left. Visible image of sharp gradient in breaking intensity at ocean front off Bodega Bay, CA, June 17, 2010. Infrared image of the sharp front in the sea surface temperature. Surface current vectors and color-coded speed with color bar in cm/s. The black line and red arrow matches with the front and arrow in the visible image (Romero et al. 2017)

The striking feature in Figure 10 is how sharp the spatial gradients are in the visible image (breaking) and IR image (temperature). In each case we estimate that the length scale of these gradients is O(10) m. While the spatial resolution of the coastal radar is only 2 km, it shows changes in surface currents across the front from approximately 20-60 cm/s or 0.4-1.2 kts. If the change in the current is small compared to the group velocity of the waves then we would expect little wave-current interaction over scales that are not large compared to the wavelength. In this case, waves of group velocity 1.2 kts have a wavelength of approximately 3.6 m, so we expect that large gradients and significant breaking over the scale of the current gradient will be limited to the shorter gravity waves, not those near the peak of the spectrum. This is consistent with the data from Romero et al. (2017).

Very recent numerical modeling and satellite remote sensing data across the Gulf Stream and in the Southern Ocean have shown that "…variations in currents at scales of 10-100 km are the main source of variations in wave heights at the same scales". (Ardhuin et al. 2017)

7. Discussion

Considerable progress has been made in better understanding the kinematics and dynamics of wind-wave breaking in the approximately thirty years since Phillips' 1985 paper. He acknowledged that his assumptions in predicting the $k^{-5/2}$ equilibrium wave spectrum are not unique. Furthermore, given the fact that S_{nl} has zero crossings, whereas S_{in} and S_{ds} are positive and negative definite, respectively, over a wide range of frequencies or

wavenumbers, his assumption that $S_{in} \propto S_{nl} \propto S_{ds}$ can only apply over a single lobe of the three in S_{nl}. Lenain & Melville (2017), using spectra like those in Figure 2 and computing S_{nl}, found that the transition wavenumber from equilibrium to saturation spectrum k_n was in the range of $(1,2)k_u$, where k_u is the zero up-crossing wavenumber going from the negative to positive lobes in S_{nl} as k increases.

This review has focused mainly on the impact of breaking on the wave field. However, breaking is the physical process by which there is a momentum flux from waves to currents, and so is very important for upper ocean dynamics and kinematics involving the vortex force due to the Eulerian vorticity and the mean Lagrangian current, which for unbroken waves includes the Stokes drift. But what is the Lagrangian drift in a breaking wave field? This was recently investigated numerically by Deike et al. (2017) who found that in breaking waves the average Lagrangian drift $\overline{u}_L \propto Sc$ significantly larger than $u_L \propto S^2 c$ for unbroken wave groups, which is consistent with Stokes classical result. With this result and the measurements of $\Lambda(c)$ we are currently investigating the contribution of breaking to the mean Lagrangian current at the ocean surface.

It has been known for some time that breaking waves contribute to air entrainment at the ocean surface and therefore to air-sea gas transfer. In a several papers the air entrainment and bubble size distribution have been considered using DNS and theoretical modeling. Deike et al. (2016) used DNS to study the air entrainment and bubble size distributions in single breaking events. Good agreement was found with the laboratory measurements of bubble size distributions (c.f. Deane & Stokes 2002) and a model based on the hypothesis that there is a balance between the buoyancy force due to the bubbles and the wave energy dissipated was successfully tested. Deike et al. (2017) went on to use the field measurements of $\Lambda(c)$ described above and the numerical results from the single breaking events to develop a model of the entrained air in the ocean that was proportional to the third moment of $\Lambda(c)$ and a function of a measure of the wave slope.

Given the inhomogeneity of breaking demonstrated in Figure 10 it is clear that this is a topic that will draw much attention in the future. One of the major trends in physical oceanography research is towards submesoscale and microscale processes at the ocean surface that contribute to vertical transport. This places an emphasis on processes at the boundaries of fronts, eddies and filaments like those visible in Figure 10. It is clear that understanding the dynamics associated with breaking will play a significant role in that research.

Acknowledgements

I wish to thank my students, postdoctoral fellows and others in my research group for making much of this work possible. They include Luc Deike, David Drazen, Laurent Grare, Jessica Kleiss, Luc Lenain, Nick Pizzo, Ron Rapp, Leonel Romero, Nick Statom, Peter Sutherland, Eric Terrill, Fabrice Veron and Chris White. My work on these topics has been supported by the physical oceanography programs at the National Science Foundation and the Office of Naval Research.

References

Agrawal, Y. C., E. A. Terray, M. A. Donelan, P. A. Hwang, A. J. Williams, W. M. Drennan, K. K. Kahma, and S. A. Kitaigorodskii (1992), Enhanced dissipation of kinetic energy beneath surface waves, *Nature*, *359*(6392), 219-220.

Alves, J., and M. L. Banner (2003), Performance of a saturation-based dissipation-rate source term in modeling the fetch-limited evolution of wind waves, *Journal of Physical Oceanography*, *33*(6), 1274-1298.

Ardhuin, F., S. T. Gille, D. Menemenlis, C. B. Rocha, N. Rascle, B. Chapron, J. Gula, and J. Molemaker (2017), Small-scale open ocean currents have large effects on wind wave heights, *Journal of Geophysical Research-Oceans*, *122*(6), 4500-4517, doi:10.1002/2016jc012413.

Banner, M.L., J. R. Gemmrich, and D. M. Farmer, 2002: Multiscale measurement of ocean wave breaking probability. J. Phys. Oceanogr.,32, 3364–3375.

Bretherton, F.P. and C. J. R. Garrett (1968), Wavetrains in inhomogeneous media, *Proceedings of the Royal Society of London Series a-Mathematical and Physical Sciences*, *302*(1471), 529-&, doi:10.1098/rspa.1968.0034.
Deane, G. B., and M. D. Stokes (2002), Scale dependence of bubble creation mechanisms in breaking waves, *Nature*, *418*(6900), 839-844, doi:10.1038/nature00967.
Deike, L., L. Lenain, and W. K. Melville (2017), Air entrainment by breaking waves, *Geophys. Res. Lett.*, *44*(8), 3779-3787, doi:10.1002/2017gl072883.
Deike, L., W. K. Melville, and S. Popinet (2016), Air entrainment and bubble statistics in breaking waves, *Journal of Fluid Mechanics*, *801*, 91-129, doi:10.1017/jfm.2016.372.
Deike, L., S. Popinet, and W. K. Melville (2015), Capillary effects on wave breaking, *Journal of Fluid Mechanics*, *769*, 541-569, doi:10.1017/jfm.2015.103.
Derakhti, M., and J. T. Kirby (2016), Breaking-onset, energy and momentum flux in unsteady focused wave packets, *Journal of Fluid Mechanics*, *790*, 553-581, doi:10.1017/jfm.2016.17.
Drazen, D. A., W. K. Melville, and L. Lenain (2008), Inertial scaling of dissipation in unsteady breaking waves, *Journal of Fluid Mechanics*, *611*, 307-332, doi:10.1017/s0022112008002826.
Duncan, J. H. (1981), An experimental investigation of breaking waves produced by a towed hydrofoil, *Proceedings of the Royal Society of London Series a-Mathematical Physical and Engineering Sciences*, *377*(1770), 331-&, doi:10.1098/rspa.1981.0127.
Gemmrich, J. (2010), Strong Turbulence in the Wave Crest Region, *Journal of Physical Oceanography*, *40*(3), 583-595, doi:10.1175/2009jpo4179.1.
Gemmrich, J. R., M. L. Banner, and C. Garrett (2008), Spectrally resolved energy dissipation rate and momentum flux of breaking waves, *Journal of Physical Oceanography*, *38*(6), 1296-1312, doi:10.1175/2007jpo3762.1.
Hasselmann, K. (1962), On the nonlinear energy transfer in a gravity-wave spectrum. 1. General theory, *Journal of Fluid Mechanics*, *12*(4), 481-500, doi:10.1017/s0022112062000373.
Jessup, A. T., and K. R. Phadnis (2005), Measurement of the geometric and kinematic properties of microscale breaking waves from infrared imagery using a PIV algorithm, *Measurement Science & Technology*, *16*(10), 1961-1969, doi:10.1088/0957-0233-16/10/011.
Kitaigorodskii, S. A., M. A. Donelan, J. L. Lumley, and E. A. Terray (1983), Wave turbulence interactions in the upper ocean. 2. Statistical characteristics of wave and turbulent components of the random velocity field in the marine surface layer, *Journal of Physical Oceanography*, *13*(11), 1988-1999, doi:10.1175/1520-0485(1983)013<1988:wtiitu>2.0.co;2.
Kleiss, J. M., and W. K. Melville (2010), Observations of Wave Breaking Kinematics in Fetch-Limited Seas, *Journal of Physical Oceanography*, *40*(12), 2575-2604, doi:10.1175/2010jpo4383.1.
Lenain, L., and W. K. Melville (2017), Measurements of the Directional Spectrum across the Equilibrium Saturation Ranges of Wind-Generated Surface Waves, *Journal of Physical Oceanography*, *47*(8), 2123-2138, doi:10.1175/jpo-d-17-0017.1.
Lighthill, J. (1978), *Waves in Fluids*, 504 pp., Cambridge University Press, Cambridge.
Longuet-Higgins, M. S. 1974 Breaking waves in deep or shallow water. In Proc. 10th Conf. on Naval Hydrodynamics, , Office of Naval Research, Dept of the Navy, ACR-204, Washington, DC, pp597-605. Melville, W. K. (1982), The instability and breaking of deep-water waves, *Journal of Fluid Mechanics*, *115*(FEB), 165-185.
Melville, W. K. (1983), Wave modulation and breakdown, *Journal of Fluid Mechanics*, *128*(MAR), 489-506.
Melville, W. K. (1994), Energy dissipation by breaking waves, *Journal of Physical Oceanography*, *24*(10), 2041-2049.
Melville, W. K., and P. Matusov (2002), Distribution of breaking waves at the ocean surface, *Nature*, *417*(6884), 58-63.
Melville, W. K., and R. J. Rapp (1985), Momentum flux in breaking waves, *Nature*, *317*(6037), 514-516.
Phillips, O. M. (1960), On the dynamics of unsteady gravity waves of finite amplitude. 1. The elementary interactions, *Journal of Fluid Mechanics*, *9*(2), 193-217.
Phillips, O. M. (1985), Spectral and statistical properties of the equilibrium range in wind-generated gravity waves, *Journal of Fluid Mechanics*, *156*, 505-531, doi:10.1017/s0022112085002221.
Phillips, O. M., F. L. Posner, and J. P. Hansen (2001), High range resolution radar measurements of the speed distribution of breaking events in wind-generated ocean waves: Surface impulse and wave energy dissipation rates, *Journal of Physical Oceanography*, *31*(2), 450-460.
Rapp, R. J., and W. K. Melville (1990), Laboratory measurements of deep-water breaking waves, *Philosophical*

Transactions of the Royal Society of London Series a-Mathematical Physical and Engineering Sciences, *331*(1622), 735-&, doi:10.1098/rsta.1990.0098.
Romero, L., L. Lenain, and W. K. Melville (2017), Observations of Surface Wave-Current Interaction, *Journal of Physical Oceanography*, *47*(3), 615-632, doi:10.1175/jpo-d-16-0108.1.
Romero, L., and W. K. Melville (2010a), Airborne Observations of Fetch-Limited Waves in the Gulf of Tehuantepec, *Journal of Physical Oceanography*, *40*(3), 441-465, doi:10.1175/2009jpo4127.1.
Romero, L., and W. K. Melville (2010b), Numerical Modeling of Fetch-Limited Waves in the Gulf of Tehuantepec, *Journal of Physical Oceanography*, *40*(3), 466-486, doi:10.1175/2009jpo4128.1.
Romero, L., W. K. Melville, and J. M. Kleiss (2012), Spectral Energy Dissipation due to Surface Wave Breaking, *Journal of Physical Oceanography*, *42*(9), 1421-1444, doi:10.1175/jpo-d-11-072.1.
Song, J. B., and M. L. Banner (2002), On determining the onset and strength of breaking for deep water waves. Part I: Unforced irrotational wave groups, *Journal of Physical Oceanography*, *32*(9), 2541-2558.
Sutherland, P., and W. K. Melville (2013), Field measurements and scaling of ocean surface wave-breaking statistics, *Geophys. Res. Lett.*, *40*(12), 3074-3079, doi:10.1002/grl.50584.
Sutherland, P., and W. K. Melville (2015a), Field Measurements of Surface and Near-Surface Turbulence in the Presence of Breaking Waves, *Journal of Physical Oceanography*, *45*(4), 943-965, doi:10.1175/jpo-d-14-0133.1.
Sutherland, P., and W. K. Melville (2015b), Measuring turbulent kinetic energy dissipation at a wavy sea surface, *Journal of Atmospheric and Oceanic Technology*, doi:10.1175/JTECH-D-14-00227.1.
Taylor, G. I. (1935), Statistical theory of turbulence, *Proceedings of the Royal Society of London Series a-Mathematical and Physical Sciences*, *151*(A873), 0421-0444, doi:10.1098/rspa.1935.0158.
Terrill, E., and W. K. Melville (1997), Sound-speed measurements in the surface-wave layer, *Journal of the Acoustical Society of America*, *102*(5), 2607-2625.
Whitham, G. B. (1965), A general approach to linear and nonlinear dispersive waves using a Lagrangian, *Journal of Fluid Mechanics*, *22*, 273-&, doi:10.1017/s0022112065000745.
Zakharov, V. E. (1968), Stability of periodic waves of finite amplitude on the surface of a deep fluid, *Journal of Applied Mechanics and Technical Physics*, *9*(2), 190-194, doi:10.1007/bf00913182.
Zappa, C. J., M. L. Banner, H. Schultz, J. R. Gemmrich, R. P. Morison,D. A. LeBel, and T. Dickey (2012), An overview of sea state conditions and air-sea fluxes during RaDyO, *J. Geophys. Res.*, *117*, C00H19, doi:10.1029/2011JC007336.